Available online at www.sciencedirect.com
ScienceDirect
Journal of Power Sources 181 (2008) 327–338
JOURNAL OF POWER SOURCES
www.elsevier.com/locate/jpowsour

Model-based optimal control of a hybrid power generation system consisting of photovoltaic arrays and fuel cells

P.L. Zervas, H. Sarimveis *, J.A. Palyvos, N.C.G. Markatos

National Technical University of Athens, School of Chemical Engineering, Zografou University Campus, 9 Heroon Polytechniou Street, GR-15780 Athens, Greece

Received 30 September 2007; received in revised form 19 November 2007; accepted 20 November 2007
Available online 28 November 2007

Abstract

Hybrid renewable energy systems are expected to become competitive to conventional power generation systems in the near future and, thus, optimization of their operation is of particular interest. In this work, a hybrid power generation system is studied consisting of the following main components: photovoltaic array (PV), electrolyser, metal hydride tanks, and proton exchange membrane fuel cells (PEMFC). The key advantage of the hybrid system compared to stand-alone photovoltaic systems is that it can store efficiently solar energy by transforming it to hydrogen, which is the fuel supplied to the fuel cell. However, decision making regarding the operation of this system is a rather complicated task. A complete framework is proposed for managing such systems that is based on a rolling time horizon philosophy.

Keywords: Hybrid systems; Renewable energy; Hydrogen; Model predictive control; Rolling horizon; Optimization

1. Introduction

Over the last few years, the limited reserves in conventional fuels like oil and the increasing interest of the public in the protection of the environment, have led the research community to seek for alternative Renewable Energy Sources (RES). Special emphasis has been given on the development and implementation of fuel-cell systems, for both academic purposes and industrial applications. Fuel cells may be considered as continuous chemical reactors which convert fuel and oxidant chemical potential into electrical energy. The key advantages of fuel cells compared to the conventional electrical power generation technologies are: higher efficiency, especially when the waste heat is used for co-generation, quiet operation suitable for residential applications, and almost zero levels of produced pollutant gases. These advantages are due to the fact that power generation in fuel cell systems is not based on combustion techniques and temperature gradients. Thus, the limitations imposed by the second law of thermodynamics on the operation of fuel cells are much less severe than the limitations imposed on conventional energy conversion systems, which are traditionally used for power generation. The most important drawback concerning fuel cell technology is that the basic fuel they use (hydrogen) does not exist free in nature [1].

A mature technology of electrical power generation from RES is the photovoltaic (PV) technology, which is characterized by zero emissions of pollutant products but, also, by low efficiency levels. However, low efficiency should not be considered as a major disadvantage, due to the zero cost of solar energy. The main disadvantage of the PV technology is that availability of solar energy is limited to daylight periods and depends on the geographical location and the weather conditions. It is obvious that solar energy cannot be stored, unless it is transformed to another type of energy. Furthermore, the accurate prediction of solar energy distribution is not feasible over a long future time horizon [2].

In order to overcome the aforementioned limitations, the concept of combining RES with hydrogen technologies emerged; and, systematic studies of this innovative type of combined systems appeared in the early 90 [3]. The term "hybrid power generation system" refers to all systems that combine different energy technologies (RES, Hydrogen, Biomass etc.) in order to meet the required electrical and thermal loads of the consumer.

* Corresponding author. Tel.: +30 210 7723237; fax: +30 210 7723138.
E-mail address: hsarimv@chemeng.ntua.gr (H. Sarimveis).

0378-7753/$ – see front matter © 2007 Elsevier B.V. All rights reserved.
doi:10.1016/j.jpowsour.2007.11.067

Nomenclature

A_i	anisotropy index
Cost	cost for purchasing electricity from the grid (€ kWh^{-1})
CostCool	cost per unit volume of H_2 for removing heat from the hydride tanks (€ Nm^{-3})
CostHeat	cost per unit volume of H_2 for adding heat to the hydride tanks (€ Nm^{-3})
CS	energy demand (kW)
eff	inverter efficiency (%)
EFG	electricity from the grid (kW)
ELIn	electrolyzer input power (kW)
ELOut	hydrogen production rate from the electrolyzer ($Nm^3\,h^{-1}$)
ETG	electricity to the grid (kW)
f	factor used to account for horizon brightening
FCIn	fuel cell hydrogen consumption ($Nm^3\,h^{-1}$)
FCOut	fuel cell power generation (kW)
GSIT	global solar irradiance on tilted surface
I_b	beam irradiance ($kW\,m^{-2}$)
I_d	diffuse irradiance ($kW\,m^{-2}$)
Inv	hydrogen stored in hydride tanks (Nm^3)
INVIn	inverter input power (kW)
INVOut	inverter output power (kW)
GSI	global solar irradiance ($kW\,m^{-2}$)
GSIT	global solar irradiance on tilted surface ($kW\,m^{-2}$)
Price	profit from selling electricity to the grid (€ kWh^{-1})
PDir	direct transferred power (kW)
PVOut	photovoltaic output power (kW)
PVsurface	net surface area of the photovoltaic array (m^{-2})
R_b	ratio of the beam irradiance on the tilted surface of the photovoltaic array to the beam irradiance on the horizontal surface
T_{amb}	ambient temperature (°C)

Greek symbols

β	slope of the photovoltaic array (°)
ρ_g	ground reflectance

Abbreviations

AGGSI	adjusted Gaussian global solar irradiance
FC	fuel cells
GSI	global solar irradiance
MINLP	mixed integer non linear programming
MPC	model predictive control
NNM	neural network model
PEM	proton exchange membrane
PV	photovoltaic
RBF	radial basis function
RES	renewable energy sources
RESHS	renewable energy system with hydrogen storage

Many researchers have focused their studies on such systems by following three main directions: (a) experimental studies on established systems; (b) simulation and optimization of their operation and (c) real time control. A number of studies [4–7] present the experimental experience which was gained during the operation of hybrid systems (solar-hydrogen, wind-hydrogen) in pilot scale. Representative references along the second direction, on the other hand, are also available [3,8–17]. Santarelli and Macagno [8], analyzed a solar-hydrogen system for a residential building in the Alps. The purpose of that system was to satisfy the complete demand in electrical energy and part of the consumer heat demand. Kelouwani et al. [9] developed a dynamic model for a stand-alone wind/solar-hydrogen system whereas Korpaas et al. [10] proposed a method for scheduling and operation of wind power plants in electricity markets. Indicative studies concerning the simulation and the optimization (in terms of choosing the optimal main components for establishing the whole system) of a renewable energy system with hydrogen storage (RESHS) are given in references [11–17]. Finally, certain references [18–20] present different methodologies of controlling hybrid renewable energy power generation systems for given load and meteorological conditions.

In this study, a novel framework is proposed for the real-time operation optimization of a solar-hydrogen power generation system. The framework is built in several steps: In the first step, a neural network model (NNM) for predicting global solar irradiance (GSI) distribution on horizontal surfaces is developed. Next step is the estimation of the electrical energy produced by the PV array. Then a model is developed that describes realistically the performance and the limitations of the hybrid system. Finally, the rolling horizon fundamental principle of Model Predictive Control (MPC) is used for developing an optimal decision strategy. In particular, an optimization problem is formulated based on the discretization of a future prediction horizon, which determines the optimal values of the decision variables at each discrete time instance. The optimization problem is reformulated and solved at each particular time instance, thus allowing the model to be updated with new information as the process progresses in time.

The rest of the paper is structured as follows: The next section describes the hybrid energy system that is studied in this work. Section 3 presents step-by-step the development of the decision making framework, from the generation of the GSI prediction model to the formulation of the complete optimization problem which provides the optimal values of the decision variables. Section 4 presents simulated results of the proposed system for a typical household and illustrates how the cost for purchasing electrical energy can be reduced. Finally, the paper ends with the concluding remarks of Section 5.

2. System description

A detailed schematic of the particular hybrid system is shown in Fig. 1. The notation used in this diagram and throughout the rest of the paper is explained in the Nomenclature.

The main components of the RESHS are the Photovoltaic Array (PV), the Electrolyzer, the Metal Hydride Tanks, the Proton Exchange Membrane Fuel Cells (PEMFC) and the inverter.

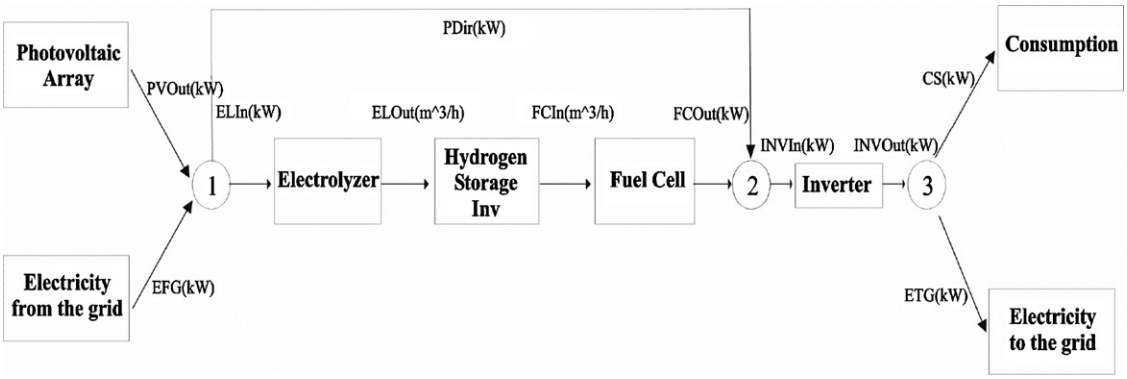

Fig. 1. Configuration of the solar-hydrogen system.

The system operates as follows: the electrical energy generated from the PV may either supply the electrolyzer – in order to produce hydrogen—or cover directly the consumer requirements. The hydrogen produced is stored in metal hydride tanks connected to a fuel cell stack. Operation of the fuel cells produces electrical energy, which is used to satisfy part or all of the consumer needs. Additionally, the system gives the opportunity to purchase electricity from the grid or sell electricity to the grid.

3. Development of the optimization procedure

In the first step, a NNM for predicting the GSI distribution on horizontal surfaces is developed. Next step is the estimation of the electrical energy produced by the PV array. Then a model is developed which realistically describes the performance and the limitations of the hybrid system. Finally, the rolling horizon fundamental principle of MPC is used for designing an optimal decision strategy.

3.1. Local prediction of the global solar irradiance

Prediction of GSI is essential for the proper design of buildings and solar energy systems. In particular, as far as PV systems are concerned, estimation of GSI and of its components (beam, diffuse, and albedo irradiance) is necessary for sizing purposes [2]. In the optimization framework described in this paper, prediction of GSI locally (where the hybrid system lies) is crucial, because it provides the necessary information for estimating the PV power generation over a future horizon. GSI is predicted using a novel methodology that is based on neural network technology and, in particular, on the Radial Basis Function (RBF) neural network architecture [21].

The GSI daily distribution is approximated by a Gaussian-type function. The RBF neural network is used to predict the parameters of the Gaussian-function (amplitude and width), using the weather state and the daylight duration as input variables. The weather conditions are categorized into discrete states, whereas the daylight duration is represented in daylight tenths. The main meteorological parameter that is used to classify the weather state is the presence and the type of clouds. In accordance with many weather-forecast models, six different states were defined for the classification of cloudiness, namely:

- State 1: Rainfall
- State 2: Heavy clouds
- State 3: Cloudy
- State 4: Partly cloudy
- State 5: Few clouds
- State 6: Clear

Fig. 2 presents characteristic daily solar irradiance distributions for all six weather states. The NNM is developed by applying the fuzzy means RBF training algorithm [22] on a database which contains local observations of the input variables (weather condition and the daylight duration) as well as the parameters of the Gaussian function over a period of time (one calendar year is strongly recommended). A correction methodology for the two tails of the Gaussian function improves further the accuracy of the produced model. The prediction model that is finally developed is named adjusted Gaussian Global solar irradiance model (AGGSI). This mathematical model is used to provide reliable future predictions of the daily GSI distributions on horizontal surfaces, given only the weather state forecast and the daylight duration. The procedure for generating an estimate of the GSI distribution for a particular day is presented graphically in Fig. 3 and is described in details in [21].

3.2. Estimation of the electrical power generation of the PV array

Assuming that the model described in the previous subsection is available, the clearness index can be calculated as the ratio of the GSI to the extraterrestrial irradiance. The latter is computed through astronomical and geographical data, given the solar constant, the day-of-year and the time-of-day. The components of GSI on the horizontal plane (beam irradiance, I_b and diffuse irradiance, I_d) are estimated next, using a correlation equation which expresses the diffuse fraction (ratio of the diffuse irradiance to the GSI) as a function of the clearness index. Among several equations that are available in the literature, the Orgill and Hollands [23] correlation was selected as the most reliable for the region of Athens, Greece. In order to estimate Global Solar Irradiance on Tilted surface (GSIT), it is necessary to employ three additional parameters: (a) the geometric factor, R_b, defined as the ratio of beam irradiance on the tilted surface of the PV array

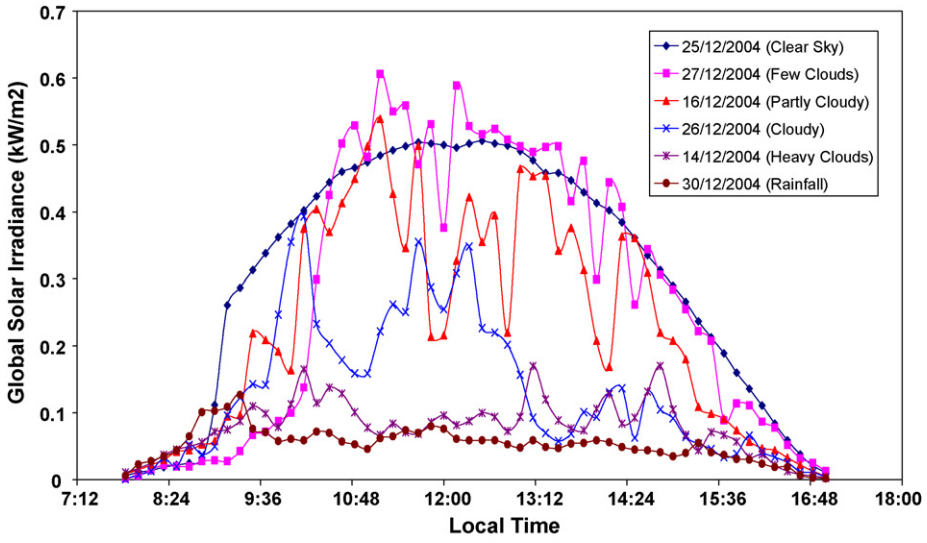

Fig. 2. Characteristic daily GSI distributions for all six weather states.

to beam irradiance on the horizontal plane; (b) the anisotropy index, A_i, which is a measure of the atmospheric transmittance of beam irradiance and is defined as the ratio of beam irradiance to the extraterrestrial irradiance, and (c) the modulating factor, f, which is used to account for "horizon brightening" and is calculated as the square root of the beam irradiance to GSI ratio. Given the ground reflectance ρ_g, and the slope of the PV array β, GSIT can be estimated through the following equation ([2], §2.16):

$$\mathrm{GSIT} = (I_\mathrm{b} + I_\mathrm{d}\, A_i) R_\mathrm{b} + I_\mathrm{d}(1 - A_i)\left(\frac{1+\cos\beta}{2}\right) \times \left(1 + f\sin^3\left(\frac{\beta}{2}\right)\right) + \mathrm{GSI}\,\rho_\mathrm{g}\left(\frac{1-\cos\beta}{2}\right) \quad (1)$$

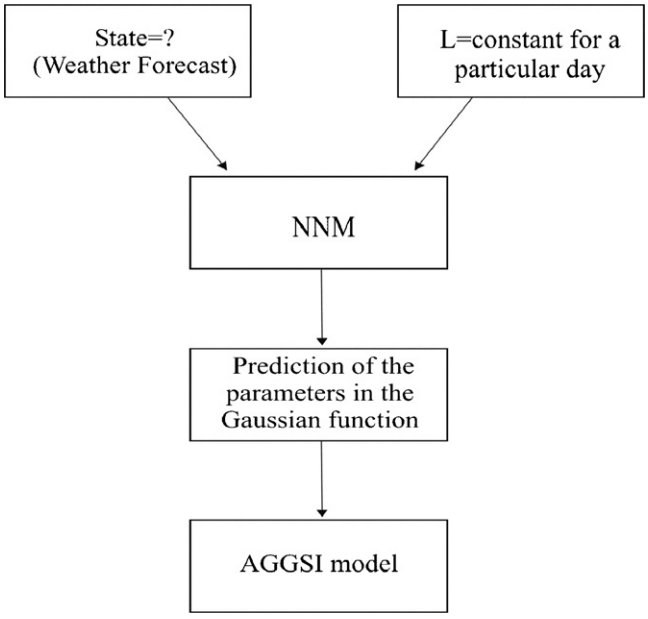

Fig. 3. The proposed algorithm for predicting the daily GSI distribution.

Finally, an empirical model is developed which expresses the photovoltaic power generation (PVOut) as a function of GSIT and the ambient temperature (T_amb), using historical data. The recorded measurements were collected during two years of operation of the Polycrystalline–Si PV arrays integrated on the southern façade and the roof of the NTUA Chemical Engineering Building [24]. The above data set was used to produce an empirical model which correlates the aforementioned quantities. Our study showed that the following linear equation provides an excellent correlation for the array DC power generation:

$$\mathrm{PVOut} = (0.128\,\mathrm{GSIT} - 0.239 \times 10^{-3}\, T_\mathrm{amb}) \times \mathrm{PVsurface} \quad (2)$$

where PVsurface is the net surface area (not including the frames of the panels) of the PV array. The units of the T_amb factor are in (kW m^{-2} °C^{-1}).

The above equation was developed and validated using a random partition of the available data into a training set and a validation set in a ratio 75%:25%. Only the training data were utilized for the development of the model and the rest of the data were used for validation purposes. The coefficient of determination R^2 (0.9909) corresponding to the validation data set is representative of the high correlation between experimental and predicted values. In order to show that the success of the model was not the result of a chance correlation, 100 different models were developed based on 100 different random partitions of the data into training and validation sets. Robustness of the model was clearly illustrated, since the coefficients of determination R^2 were over 0.989 for all 100 partitions.

In conclusion, PVOut can be predicted locally over a future time horizon given only standard weather forecast information (weather state and ambient temperature). According to the produced mathematical model, the effect of the ambient temperature on the PV performance is negative (i.e when this temperature increases, the efficiency of the array drops). This observation agrees with the results that have been reported in the litera-

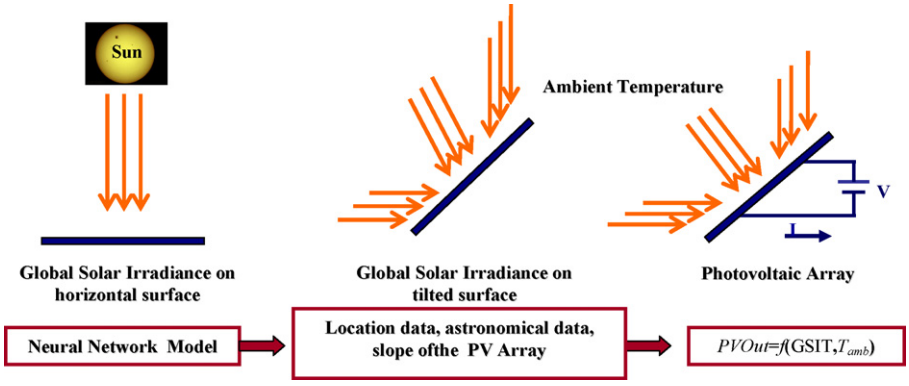

Fig. 4. Estimation of PV power generation.

ture (cf. [2], ch. 23). Fig. 4 illustrates the procedure used for estimating the PV power generation over a future time horizon.

3.3. Estimation of the inverter efficiency

The inverter efficiency is a function of the normalized input power, i.e. the ratio of the inverter input power to the nominal input capacity. However, for normalized input power greater than 15%, the efficiency for most commercial inverters is close to 0.9, as it is verified by the manufacturer specifications. In our model, we assume that the inverter efficiency is constant over the entire range of normalized input power. This assumption is also used in the popular TRNSYS simulator [25]. In order to compute experimentally an estimate of the inverter efficiency, we used again historical data that were collected over the course of two years operation from a commercial inverter located in the Solar Engineering Unit of Chemical Engineering School at NTUA [24]. The estimated efficiency was found equal to 89.3%. The result was validated using the same procedure that was described in the previous subsection, i.e. by partitioning the data into training and validation sets in a ratio 75%:25%. We generated 100 different random partitions and in all of them the coefficient of determination R^2 was over 0.99.

3.4. Development of the mass and electrical energy balance

The two main processes of the hybrid system occur in the electrolyzer and the fuel cells, while the hydride tanks serve as storage units. The inverter efficiency is also taken into account in the development of the equations that are presented in this subsection. Using the notation CS(k), EFG(k), ELIn(k), ELOut(k), ETG(k) FCIn(k), FCOut(k), INVIn(k), INVOut(k), PDir(k), PVOut(k), to denote the integrated values of the variables introduced in Fig. 1 over the length of a particular time period k and the notation Inv(k) for the hydrogen inventory level at the end of period k, we can write the relevant equations.

3.4.1. Electrolyzer and fuel cell performance equations

Manufacturers of electrolyzers provide the necessary data to generate equations that express the power consumed by the electrolyzer as a function of the produced rate of hydrogen. Similarly, for fuel cell systems equations can be developed that relate the produced power with the consumed rate of hydrogen. These equations take into account the parasitic loads, which are due to the auxiliary subunits in each particular system. The equations differ between manufacturers, so at this point we use generic functions to denote the existence of such mathematical relationships.

$$\mathrm{ELIn}(k) = L_1(\mathrm{ELOut}(k)) \tag{3}$$

$$\mathrm{FCOut}(k) = L_2(\mathrm{FCIn}(k)) \tag{4}$$

3.4.2. Hydrogen mass balance

The hydrogen inventory level at the end of period k is equal to the inventory level at the end of the previous time period, plus the amount of hydrogen produced by the electrolyzer during period k minus the quantity of hydrogen consumed by the fuel cell during the same period.

$$\mathrm{Inv}(k) = \mathrm{Inv}(k-1) + \mathrm{ELOut}(k) - \mathrm{FCIn}(k) \tag{5}$$

3.4.3. Overall electrical energy balance

The overall electrical energy balance takes into account all the different areas in the system where energy is generated or consumed. In order to arrive to this equation, we first write electrical energy balance equations at nodes 1, 2, 3, which are indicated in Fig. 1.

Energy balance at node 1 :

$$\mathrm{PVOut}(k) + \mathrm{EFG}(k) = \mathrm{ELIn}(k) + \mathrm{PDir}(k) \tag{6}$$

Energy balance at node 2 : $\mathrm{PDir}(k) + \mathrm{FCOut}(k) = \mathrm{INVIn}(k)$ (7)

Energy balance at node 3 : $\mathrm{INVOut}(k) = \mathrm{CS}(k) + \mathrm{ETG}(k)$ (8)

If we additionally assume a constant efficiency inverter eff, as indicated in the previous subsection, i.e.

$$\mathrm{INVOut}(k) = \mathrm{eff} \times \mathrm{INVIn}(k) \tag{9}$$

then from Eqs. (6)–(9) we can easily derive the following overall electrical energy balance equation.

$$\mathrm{eff} \times (\mathrm{PVOut}(k) + \mathrm{EFG}(k) + \mathrm{FCOut}(k) - \mathrm{ELIn}(k)) = \mathrm{CS}(k) + \mathrm{ETG}(k) \tag{10}$$

3.5. Formulation of the optimization problem

MPC has recently advanced to a popular control methodology for industrial and process applications. Its wide adoption from the industry is largely based on the inherent ability of the method to handle efficiently constraints and uncertainties in multivariable dynamical systems. MPC is based on the following simple idea: at each discrete time instance the control action is obtained by solving on-line a finite-horizon open-loop optimal control problem, using the current state of the system as the initial state. A finite-optimal control sequence is obtained, from which only the first element is actually applied to the system. The procedure is repeated after each state transition.

The fundamental rolling horizon principle of MPC is used in this work to design an optimal-decision strategy for the RESHS. The model developed in the previous subsection is extended to account for the future time periods, while the estimated profiles of the electrical energy produced by the PV array and the energy demand provide the input information. An optimization problem is formulated based on the discretization of the future time horizon. The solution of the optimization problem provides the optimal values of the decision variables over the future horizon. The key decision variables are: the energy which is supplied to the electrolyser, the energy purchased or sold to the grid during each future time period, and the quantity of hydrogen stored in the hydride tanks at the end of each time period. The adoption of the rolling horizon principle means that only the optimal values associated with the first future time period are actually applied to the system. The model is updated with new information as the process progresses with time and the optimization problem is reformulated and solved at each particular discrete time instance.

Assuming a number of P equally spaced future time intervals, the precise formulation of the optimization problem is as follows:

Objective function:

$$\min \sum_{i=1}^{P} \begin{bmatrix} \mathrm{EFG}(k+i) \times \mathrm{Cost}(k+i) - \mathrm{ETG}(k+i) \times \mathrm{Price}(k+i) \\ +\mathrm{Inv}\,U(k+i) \times \mathrm{CostCool} + \mathrm{Inv}\,D(k+i) \times \mathrm{CostHeat} \end{bmatrix} \tag{11}$$

Constraints:

$$\begin{aligned} &\text{If} \quad \mathrm{Inv}(k+i) - \mathrm{Inv}(k+i-1) \geq 0 \\ &\text{then} \quad \mathrm{Inv}\,U(k+i) = [\mathrm{Inv}(k+i) - \mathrm{Inv}(k+i-1)], \\ &\qquad i = 1, \ldots, P \end{aligned} \tag{12}$$

$$\begin{aligned} &\text{If} \quad \mathrm{Inv}(k+i) - \mathrm{Inv}(k+i-1) < 0 \\ &\text{then} \quad \mathrm{Inv}\,D(k+i) = [\mathrm{Inv}(k+i-1) - \mathrm{Inv}(k+i)], \\ &\qquad i = 1, \ldots, P \end{aligned} \tag{13}$$

$$\mathrm{ELIn}(k+i) = L_1(\mathrm{ELOut}(k+i)), \quad i = 1, \ldots, P \tag{14}$$

$$\mathrm{FCOut}(k+i) = L_2(\mathrm{FCIn}(k+i)), \ i = 1, \ldots, P \tag{15}$$

$$\mathrm{Inv}(k+i) = \mathrm{Inv}(k+i-1) + \mathrm{ELOut}(k+i) - \mathrm{FCIn}(k+i), \quad i = 1, \ldots, P \tag{16}$$

$$\begin{aligned} &\mathrm{eff} \times (\mathrm{PVOut}(k+i) + \mathrm{EFG}(k+i) + \mathrm{FCOut}(k+i) \\ &\qquad -\mathrm{ELIn}(k+i)) = \\ &\mathrm{CS}(k+i) + \mathrm{ETG}(k+i), \ i = 1, \ldots, P \end{aligned} \tag{17}$$

$$\text{If} \quad \mathrm{EFG}(k+i) > 0 \quad \text{then} \quad \mathrm{ETG}(k+i) = 0, \quad i = 1, \ldots, P \tag{18}$$

$$\text{If} \quad \mathrm{ETG}(k+i) > 0 \quad \text{then} \quad \mathrm{EFG}(k+i) = 0, \quad i = 1, \ldots, P \tag{19}$$

Eq. (11) is the objective function to be minimized, which actually represents the cost for purchasing electricity during the future time horizon minus the corresponding profit of selling electricity to the grid. Cost$(k+i)$ and Price $(k+i)$ represent the cost per unit and profit per unit of purchasing/selling electricity from/to the grid within time period $k+i$. Thus, the system is able to take into account situations where electricity prices vary from period to period (consider for example the different day and night electricity rates). The objective function also takes into account the cost for removing heat from the hydride tanks during addition of hydrogen and the cost for adding heat to the tanks during extraction. The cost is considered proportional to the amount of hydrogen Inv$U(k+i)$/Inv$D(k+i)$ added to or extracted from the hydride tanks. In particular the amount of hydrogen added during a time interval is multiplied by CostCool, while the amount of hydrogen removed is multiplied by CostHeat, where CostCool and CostHeat represent the cost per unit volume of hydrogen for removing/adding heat to the hydride tanks. As far as the constraints are concerned, Eqs. (12) and (13) compute the amounts of hydrogen added or subtracted from the hydride tanks during time intervals, which are used in the objective function. Eqs. (14)–(17) are extensions of Eqs. (3)–(5), (10) for the entire future time horizon. Eqs. (18) and (19) prevent the system from purchasing and selling electrical energy to the grid during the same time interval. In addition to the above constraints, the variables are bounded between upper and lower limits to account for process limitations. PVOut$(k+i)$, ELin$(k+i)$, ELOut $(k+i)$, FCIn$(k+i)$ and FCOut$(k+i)$ are bounded from above by the production capacities of the PV array, the electrolyzer and the fuel cell system, while Inv$(k+i)$ is bounded from above by the storage capacity of the hydride tanks. All the variables are obviously bounded from below by zero. Alternatively, we can impose greater-than-zero lower bounds to prevent the system components from operating at very low production rates and the hydrogen inventory level from going below a safe threshold value. Additional constraints may be included in the optimization problem, according to each particular situation.

Remark: The optimization problem described by Eqs. (11)–(19) and the upper and lower bounds on the decision variables is a complex nonlinear programming problem. Eqs. (12)–(13) and (18)–(19) have been presented in an intuitive form. However insertion of the if-then statements in mathematical programming solvers is not allowed or may cause computational flows. The same equations can be formulated so that they do not make use of if-then statements, by introducing sets of binary

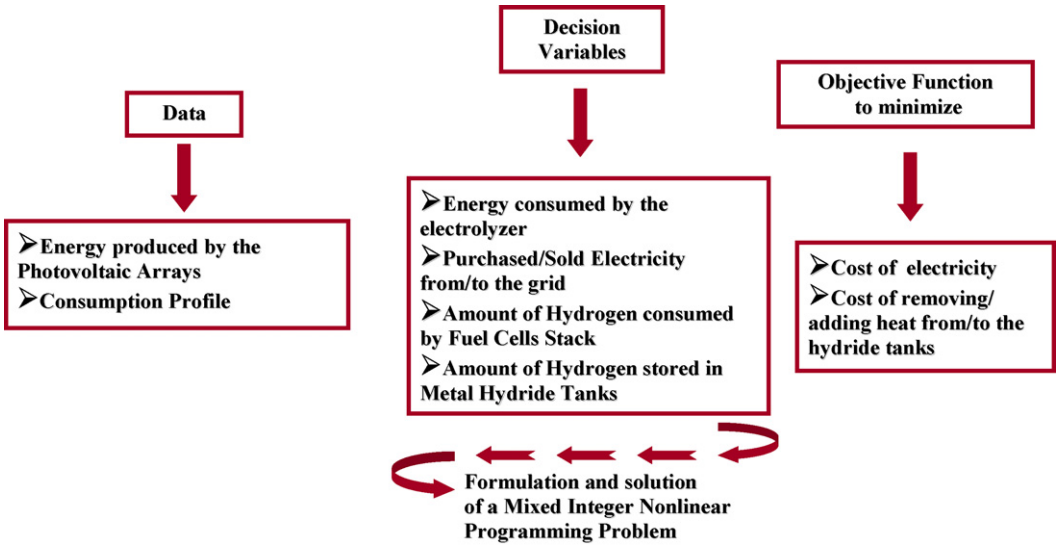

Fig. 5. Formulation of the optimization problem applied to the RESHS.

variables. In particular, Eqs. (12) and (13) can be formulated as follows:

$$\begin{aligned} &\mathrm{Inv}(k+i) - \mathrm{Inv}(k+i-1) = \mathrm{Inv}\,U(k+i) - \mathrm{Inv}\,D(k+i), \quad i = 1, \ldots, P \\ &\mathrm{Inv}\,U(k+i) \le M_1 \times \mathrm{IC}(k+i), \qquad i = 1, \ldots, P \\ &\mathrm{Inv}\,D(k+i) \le M_1 \times \mathrm{IH}(k+i), \qquad i = 1, \ldots, P \\ &\mathrm{IC}(k+i) + \mathrm{IH}(k+i) = 1, \qquad i = 1, \ldots, P \end{aligned} \tag{20}$$

where M_1 is a fixed big positive number (the storage capacity of the hydride tanks) and IC($k+i$), IH($k+i$), I=1,. . .,P are binary variables.

Similarly, Eqs. (18) and (19) can be written in the following form

$$\begin{aligned} &\mathrm{EFG}(k+i) \le M_2 \times \mathrm{IP}(k+i), \qquad i = 1, \ldots, P \\ &\mathrm{ETG}(k+i) \le M_2 \times \mathrm{IS}(k+i), \qquad i = 1, \ldots, P \\ &\mathrm{IP}(k+i) + \mathrm{IS}(k+i) = 1, \qquad i = 1, \ldots, P \end{aligned} \tag{21}$$

where M_2 is a fixed big positive number (an upper bound on the amount of energy that may be purchased/sold from/to the grid during a time interval) and IP($k+i$), IS($k+i$), i = 1,. . .,P are additional sets of binary variables.

Using the formulations described by Eqs. (20) and (21) in place of Eqs. (12)–(13) and (18)–(19) a Mixed Integer Nonlinear Programming problem (MINLP) is generated. The problem is solved using GAMS [26], which is a powerful commercial modelling language. The formulation of the optimization problem is described graphically in Fig. 5.

4. Results

In this section, simulation results are presented, concerning the application of the proposed method in optimizing the performance of a RESHS, which is used to cover the energy needs of a typical household located in Athens, Greece. Based on recorded data, reference energy consumption daily profiles were created for each month. Fig. 6 shows the reference profile for October, which will be used for the simulations that follow in the sequel.

Future predictions of the electrical energy produced by the PV array are based on a GSI prediction model, which was developed as described in Section 3.2. For the development of the model, we used data that have been recorded over the course of two years by the meteorological station located at the NTUA campus, Athens, Greece. Fig. 7 shows the prediction of the PVOut three-day-profile available at the beginning of the simulation. The PVOut prediction corresponds to the sequence is 4 → 5 → 4, i.e. partly cloudy weather conditions for the first day, few clouds conditions for the second day and partly cloudy conditions for the third day. The equations concerning the electrolyzer and the fuel cells have been provided by a manufacturer located in Greece [27]. The equations take into account the parasitic loads that are present due to the auxiliary subunits in each particular system.

$$\begin{aligned} \mathrm{ELIn}(k) = {} & 3.348\,\mathrm{ELOut}(k) + 1.367 \ln\left(\frac{\mathrm{ELOut}(k)}{104.621}\right) \\ & + 3.845 \times 10^{-5}\,\mathrm{ELOut}(k)^2 \end{aligned} \tag{22}$$

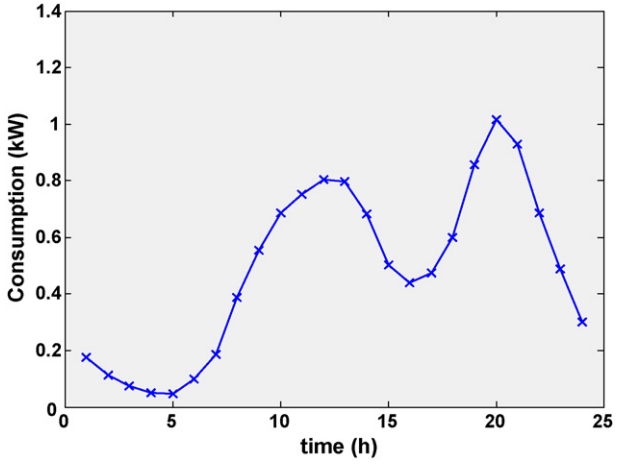

Fig. 6. Reference load profile for October reference.

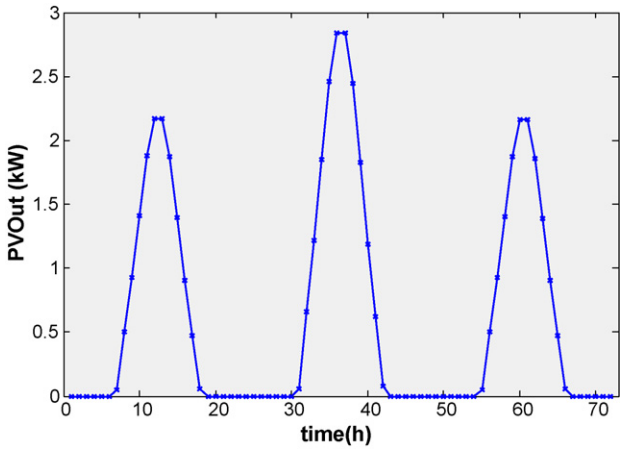

Fig. 7. Prediction of the PV output three-day-profile.

Table 1
Hybrid system specifications

	First scenario	Second scenario
PV array	4 kWp	4 kWp
Electrolyzer	0.25 $Nm^3\,h^{-1}$	0.5 $Nm^3\,h^{-1}$
Fuel cell stack	1.2 kW	1.2 kW
Metal hydride tanks	5 Nm^3	5 Nm^3

$$\mathrm{FCOut}(k) = -0.273 \times 10^{-9}\,\mathrm{FCIn}(k)^4 + 7.726 \times 10^{-7}\,\mathrm{FCIn}(k)^3 - 0.916 \times 10^{-3}\,\mathrm{FCIn}(k)^2 + 1.745\,\mathrm{FCIn}(k) \quad (23)$$

As explained in Section 3.3 the inverter efficiency is assumed constant and equal to 89.3%. The cost for purchasing electrical energy is 0.09 € kWh^{-1} whereas it is assumed that the profit from selling electrical energy to the grid is 0.05 € kWh^{-1}. A lower bound of 1 Nm^3 (20% of the hydride tanks storage capacity) is imposed on the hydrogen inventory level. Due to the fact that we use hydride tanks of small sizes in our simulations, the cost for removing or providing heat to the tanks is assumed negligible and therefore that parameters CostCool and CostHeat are set equal to zero.

Two scenarios regarding the specification of the RESHS were simulated. The particular details are summarized in Table 1 which shows the production capacities of the three main processes (PV array, electrolyzer, fuel cell) and the storage capacity of the metal hydride tanks. The only difference between the two scenarios is the maximum production rate of the electrolyzer, which is lower in the first scenario. As initial and final values for the hydrogen inventory level, 50% and 20% of the storage capacity were assumed in both scenarios.

Fig. 8 presents graphically the solutions of the optimization problems which were formulated for the two scenarios. The solutions are presented in the form of optimal profiles (plots (a)–(h)) of all input and output variables over the future time horizon of 72 h. The first scenario is represented by green lines and the second scenario by blue lines.

Regarding the first scenario, we notice that during the hours of peak generation of electrical energy from the PV array, the electrolyzer operates close to its maximum production rate. During the same period, electricity from the grid is zero whereas the surplus is sent to the grid. Furthermore, a gradual filling of the tanks with hydrogen is observed due to the operation of the electrolyzer. This inventory build-up is used for producing electricity in the fuel cell at subsequent periods when there is high energy demand but low or zero generation of electrical energy from the PV array. So, in the evening hours, when energy demand is high but solar energy is no longer available, the demand is mainly fulfilled by the fuel cells, while small amounts of electrical energy are purchased from the grid. Comparing the optimal profiles of the two scenarios, it is clear that the specification is critical for the performance of the RESHS. Due to the increased production capacity of the electrolyzer, the cost for purchasing electrical energy from the grid is lower in the second scenario. Table 2 summarizes the results for the first scenario regarding the amounts of energy that are purchased from the grid or sold throughout the entire time horizon and the corresponding objective function value.

In the results presented so far, we have assumed that the temporal profiles of the input variables (i.e. PVOut and CS) are deterministic, i.e. their true values match exactly the initial predictions throughout the prediction horizon. Obviously, perfect prediction cannot be achieved in real-life applications. In order to examine this issue, we generated modified CS temporal profiles by introducing noise to the available predictions whereas for the PVOut we used true profiles as they have been recorded for three subsequent days in October. In particular, the value of $CS(k+i)$, at each future time instance $i = 1,\ldots,P$ was distorted by adding a random number, chosen from a uniform distribution in the interval $[-0.1\cdot CS(k+i)\ 0.1\cdot CS(k+i)]$. Regarding the true PVOut values, the recorded data [24] for the three subsequent days correspond to partly cloudy (state 4), clear sky (state 6) and heavy clouds (state 2) conditions respectively. Fig. 9 presents the PVOut recorded data and the modified CS profile together with the available predictions. It is clear that as far as PVOut is concerned, we introduce systematic error to the available predictions, which increases with the period into the future.

Table 2
Purchased/sold energy and objective-function value using deterministic and updated decision strategies

	Total energy from the grid (kWh)	Total energy to the grid (kWh)	Objective function (€)
Deterministic schedule using predicted PVOut and CS temporal profiles	9.7808	4.9563	0.63
Deterministic schedule using true PVOut and CS temporal profiles	27.8317	17.2793	1.64
Updated schedule using true PVOut and CS temporal profiles	13.2176	7.9778	0.79

Given the difference between true and predicted PVOut and CS profiles, an obvious question emerges: how might this discrepancy deteriorate the efficiency of the decision policy that was obtained as the solution to the deterministic optimization problem? In order to answer that question, we used again the deterministic schedule that was determined for Scenario 1, but now considering the true instead of the simulated PVOut and CS temporal signals. During each time period additional shortages of energy were satisfied by purchasing it from the grid, while additional surpluses of energy were sold to the grid. The results are shown with green lines in Fig. 10. The amounts of energy that are purchased from the grid or sold throughout the entire time horizon are shown in Table 2 and compared with those obtained when zero noise was assumed. Clearly, both quantities are considerably higher when the true temporal PVOut and CS profiles are taken into consideration. The total cost (value of the objective function) increases substantially (160%). This observation actually means that efficiency becomes lower when the sched-

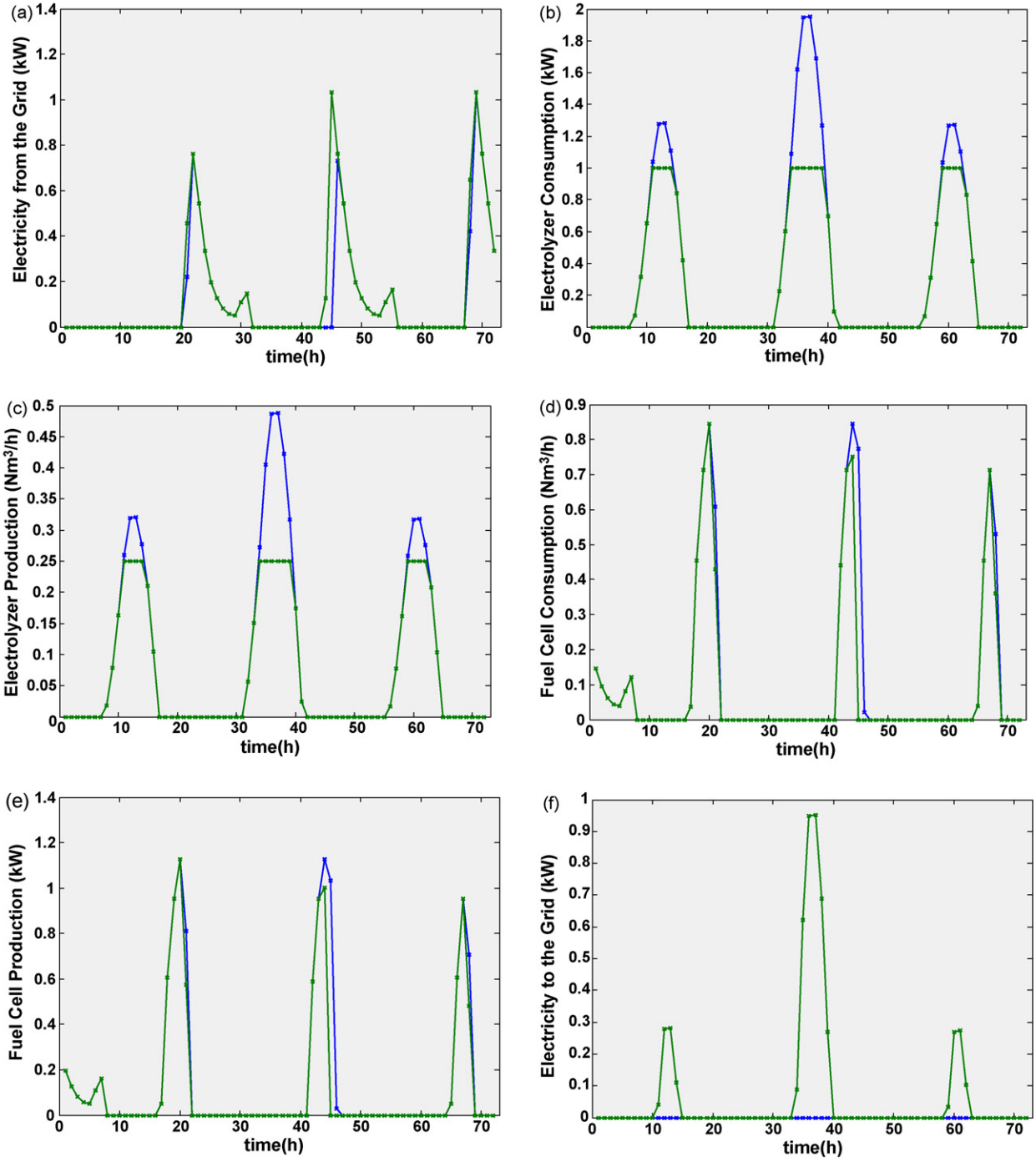

Fig. 8. Decision strategy for two different scenarios of a RESHS: (a) electricity from the grid; (b) electrolyzer consumption; (c) electrolyzer production; (d) fuel cell consumption; (e) fuel cell production; (f) electricity to the grid; (g) direct transferred power and (h) inventory (scenario 1 and scenario 2 are represented by green and blue lines, respectively). (For interpretation of the references to color in this figure legend, the reader is referred to the web version of the article.)

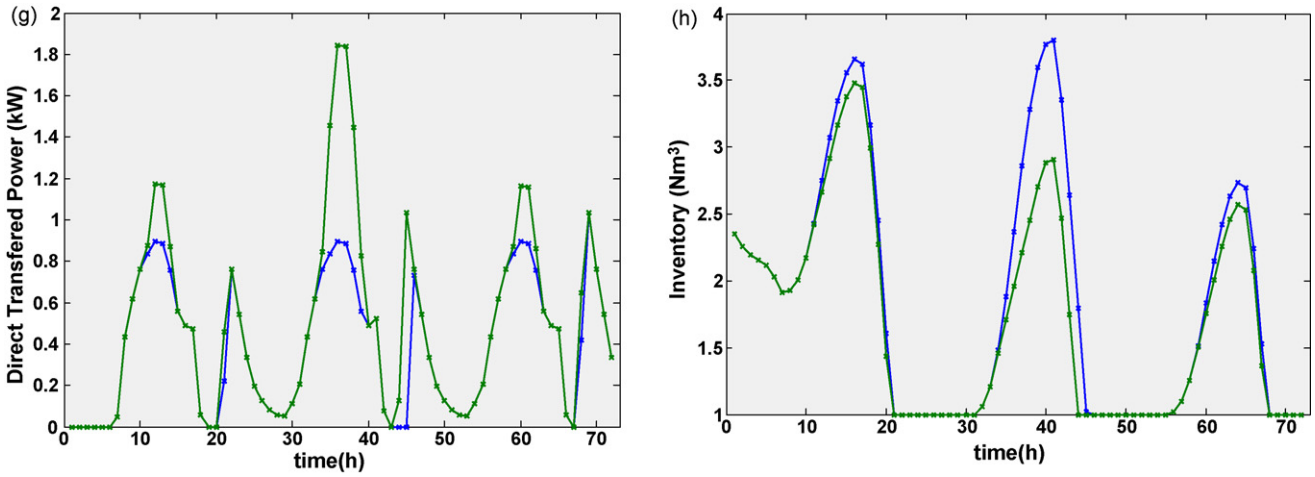

Fig. 8. (*Continued*).

ule obtained from the solution of the deterministic optimization problem is applied to realistic situations containing noisy PVOut and CS temporal profiles.

In the rest of the section, we will explore the benefits of using the rolling horizon concept for improving the decision strategy that has been determined so far. The rolling horizon philosophy is based on the fact that at each discrete time instance, the formulation of the optimization problem can be updated with the true current state of the system (the hydrogen inventory level) and with more reliable predictions regarding the future PVOut and CS temporal profiles. In our particular application, we assume that at each time instance we know the true values of PVOut and CS only for the next time period, while for the rest of the future horizon we keep using the initial PVOut and CS predictions. This assumption is rather conservative, since in real life situations we can most probably improve our predictions for the entire future time horizon. However, as we will see in the sequel, our assumption is good enough for demonstrating the effectiveness of the rolling horizon strategy.

Following the previously described information update procedure at the end of each discrete time period, the complete optimization problem is reformulated and solved. The optimal control strategy resulting from the rolling horizon philosophy is shown in red lines in Figure 10, where we can compare it with the decision strategy produced by the solution to the deterministic problem (shown in green lines). We observe slight modifications in the electrolyzer operation schedule for the first two days and major modifications during the third day. For the fuel cell system considerable modifications are observed, which result to a quite different inventory temporal profile and to reduced amounts of purchased and sold electricity (see Table 2). The total cost is quite close to the one calculated by using the predicted and not the actual PVOut and CS temporal profiles (there is only a 25% increase). It is also useful to compare this result with the cost for covering all the consumer needs by purchasing electrical energy from the grid, which is 3.16 € (i.e. only 25% of the consumer needs is covered by purchasing electrical energy from the grid). Therefore, the adoption of the rolling horizon concept can improve considerably the efficiency of the hybrid system in real-life situations, where PVOut and CS predictions obviously contain errors.

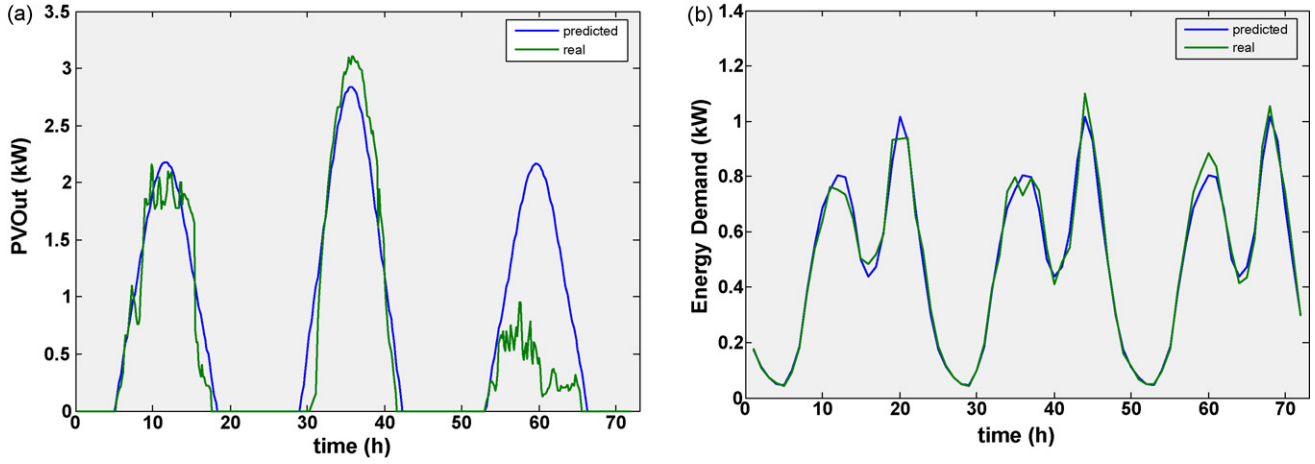

Fig. 9. True and predicted temporal profiles for (a) PVOut and (b) CS.

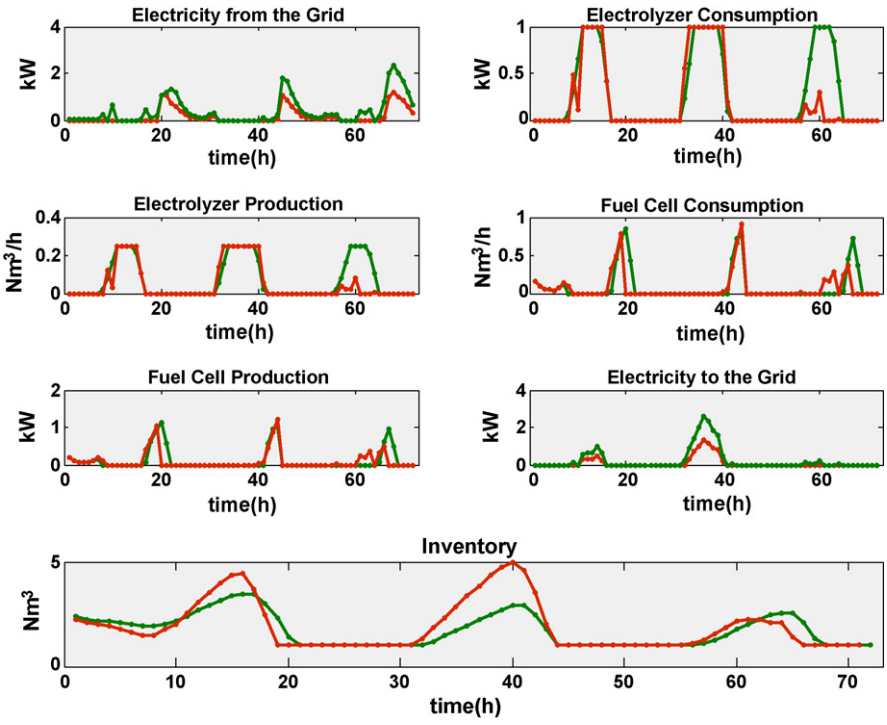

Fig. 10. Deterministic and updated decision strategies for scenario 1 with true PVOut and CS profiles (deterministic and updated decision strategies are represented by red and green lines respectively). (For interpretation of the references to color in this figure legend, the reader is referred to the web version of the article.)

5. Conclusions

In this work, a complete framework for managing renewable energy systems with hydrogen storage is proposed. The framework is built in several steps that may be summarized as follows:

- Development of a prediction model for the GSI daily profile on horizontal surfaces based on the RBF neural network architecture;
- Forecasting GSI on the tilted surface of the PV array, using the following information: the GSI prediction on horizontal surfaces, astronomical and geographical data and the slope of the PV array;
- Estimating the electrical energy produced by the PV array, given the ambient temperature and the GSI on the tilted surface;
- Development of a model that realistically describes the performance and the constraints of the hybrid system;
- Formulation and solution of an on-line optimization problem that is used as a decision making tool regarding the operation of the system. The formulation takes into account updated estimations of the photovoltaic power generation over a future prediction horizon and a profile of the energy demand over the same time horizon.

In conclusion, the proposed model may prove to be a very useful tool for optimal decision making in hybrid power generation systems which combine RES and hydrogen technologies. It should also be mentioned that the actual cost of all individual components of such a hybrid system is continuously decreasing, since renewable energy technologies become mature. Hybrid renewable energy systems are expected to be competitive to the conventional power generation systems in the near future and thus optimization of their operation is of particular interest.

References

[1] J. Larminie, A. Dicks, Fuel Cell Systems Explained, second ed., John Wiley & Sons Ltd., New York, 2003.
[2] J.A. Duffie, W.A. Beckman, Solar Engineering on Thermal Processes, third ed., John Wiley & Sons Ltd., New York, 2006.
[3] P.D. Lund, Int. J. Hydrogen Energ. 16 (1991) 735–740.
[4] R. Gazey, S.K. Salman, D.D. Aklil-D'Halluin, J. Power Sources 157 (2006) 841–847.
[5] A.M. Chaparro, J. Soler, M.J. Escudero, E.M.L. de Ceballos, U. Wittstadt, L. Daza, J. Power Sources 144 (2005) 165–169.
[6] P.C. Ghosh, B. Emonts, H. Janćen, J. Mergel, D. Stolten, Sol. Energ. 75 (2003) 469–478.
[7] J.P. Vanhanen, P.S. Kautranen, P.D. Lund, Int. J. Hydrogen Energ. 22 (1997) 707–713.
[8] M. Santarelli, S. Macagno, Energ. Convers. Manage. 45 (2004) 427–451.
[9] S. Kelouwani, K. Agbossou, R. Chahine, J. Power Sources 140 (2005) 392–399.
[10] M. Korpaas, A.T. Holena, R. Hildrum, Electr.Power Energ. Syst. 25 (2003) 599–606.
[11] M.J. Khan, M.T. Iqbal, Renew. Energ. 30 (2005) 835–854.
[12] L. Ntziachristos, C. Kouridis, Z. Samaras, K. Pattas, Renew. Energ. 30 (2005) 1471–1487.
[13] E. Kasserisa, Z. Samarasa, D. Zafeiris, Renew. Energ. 32 (2007) 57–79.
[14] M.T. Iqbal, Renew. Energ. 28 (2003) 511–522.
[15] Jun-Hai Shi, Xin-Jian Zhu, Guang-Yi Cao, Int. J. Energ. Res. 31 (2007) 315–328.
[16] M. Santarelli, D. Pellegrino, Renew. Energ. 30 (2005) 493–510.
[17] M. Santarelli, M. Cali, S. Macagno, Energy 29 (2004) 1159–1182.
[18] A. Bilodeau, K. Agbossou, J. Power Sources 162 (2006) 757–764.

[19] H. De Battista, R.J. Mantzb, F. Garellia, J. Power Sources 155 (2006) 478–486.
[20] A. Al-Alawia, S.M. Al-Alawib, S.M. Islam, Renew. Energ. 32 (2007) 1426–1439.
[21] P.L. Zervas, H. Sarimveis, J.A. Palyvos, N.C.G. Markatos, Renew. Energ. 33 (2008) 1796–1803.
[22] H. Sarimveis, A. Alexandridis, G. Tsekouras, G. Bafas, Ind. Eng. Chem. Res. 41 (2002) 751–759.
[23] J.F. Orgill, K.G.T. Hollands, Sol. Energ. 9 (1977) 357–359.
[24] http://www.chemeng.ntua.gr/solarlab/THERMIE-en.html.
[25] Klein et al., 2000. TRNSYS 15, A Transient Simulation, Program. Solar Energy Laboratory, University of Wisconsin, Madison, Wisconsin, WI, USA.
[26] Brooke A, Kendrick D, Meeraus A, Raman R. GAMS, User Guide. Available with the GAMS system or from http://www.gams.com; 1998.
[27] Private Communication 29.10.2007, Tropical SA, 2007.